Print ISSN 2710-0200 *Full text available online at* *Ethiop J Nat Comp Sci.*
Electronic ISSN 2710-0219 *http://journal.uog.edu.et/index.php/EJNCS* *Vol. 4 (2) 550-568*
https://doi.org/*10.20372/ejncs/Ma.2024.011*

ORIGINAL RESEARCH

Effects of Homogeneous-Heterogeneous Reactions in Flow of Electrical MHD Non-Newtonian Fluid with a Rotating Frame: An Analytical Approach

Gossaye Aliy Adem

Department of Mathematics, University of Gondar, Gondar, Ethiopia
gosyy610@gmail.com, gossaye.aliy@uog.edu.et

Received: 9 March 2023 / Accepted: 2 July 2024 / Published: 29 August 2024

Abstract

This work provides an analytical method for the rotational flow of an electrical MHD Maxwell fluid that is limited by an elastic sheet that deforms linearly. Analysis of mass transfer is completed in the presence of HHR. The standard transformation is applied to translate the governing equations into similarity equations, which are then solved by the OHAM (optimal homotopy asymptotic technique). We have found that the OHAM technique works well, consistent, dependable, and efficient when it comes to solving highly nonlinear differential equations. For a certain range of Maxwell fluid parameters, concentration and velocity profiles are computed and explained. The rotation-strength parameter λ has a significant impact on the flow fields. The velocity curves are an oscillatory fading function of the dimensionless vertical distance for large values of λ. In the presence of an electric field, increasing the magnetic field first causes the velocity field to decrease, but eventually it starts to increase noticeably. As chemical reaction strengths increase, the concentration distribution at the sheet is observed to decrease. The current calculations are compared to those of previously published studies, and the results seem credible.

Keywords: OHAM, Electric field, Chemical reaction, Rotating frame, Maxwell fluid

Introduction

Fluids which are non-Newtonians convert their flow behavior or viscosity under stress. Illustrative examples are food products, polymer solutions, fibers in liquid paper pulp, molten plastics, emulsions of water in oil, etc. Maxwell fluids are special kind of non-Newtonian fluids which reveal an added feature of elasticity apart from viscosity, that is, they have the capacity to store and recover shear energy. Maxwell fluid is a common viscoelastic model that can forecast stress relaxation occurrence for a variety of polymeric liquids. HT and MHD flow for Maxwell fluid with variable thermal conductivity over a surface which is exponentially stretching were addressed by Singh and Agarwal.

Non-Newtonians fluids change their viscosity or flow characteristics when under stress. Food items, polymer solutions, the fibers in liquid

paper pulp, molten polymers, water-in-oil emulsions, etc. are some instances that serve as illustrations. A unique class of non-Newtonian fluids known as Maxwell fluids exhibit the ability to store and recover shear energy, a characteristic of elasticity in addition to viscosity. A popular viscoelastic model that can predict the onset of stress relaxation in a range of polymeric liquids is the Maxwell fluid. Singh and Agarwal (Singh and Agarwalb, 2014) investigated HT and MHD flow for Maxwell fluid with changing thermal conductivity across an increasingly stretched surface. Waini *et al.* (2017) discussed the associated magnetic field impacts on HT and the flow of the upper-convected Maxwell fluid. The impacts of heat sink/source and chemical reaction on MHD Maxwell nanofluid flow over a heated surface was analytically solved by Sravanthi and Gorla, (2018). Agbaje and Leach (2020) investigated numerically the impact of heat generation, thermal radiation and chemical reaction on vertical permeable flat plate for the Jeffrey nanofluid flow. Considerable research in this area has been published by many researchers (see, for instance, (Khan *et al.*, 2016; Hsiao, 2017; Ali *et al.*, 2018)).

Numerous applications in science, engineering, and geophysics include rotating fluid flow problems. Food processing, vacuum cleaners, pumps, jet engines, chemical processes, solidification, centrifugal casting of metals, and rotating gear are a few significant technical uses. Rotating flows around constantly deforming sheets have received a lot of interest recently. The first work in this subject was reported by Wang (1988) ,who investigated the FF across a stretching sheet immersed in a rotating Newtonian fluid. Subsequently, Nazar et al. (Nazar, Amin and Pop, 2004) used numerical methods for velocity profiles to expand Wang's investigation for unstable fluid flow scenarios. Kumari *et al*. (2006) investigated the rotational flow of a non-Newtonian power-law fluid across a stretchy sheet. The 3D rotating flow of Jeffrey fluid for the Cattaneo-Christov heat flux model was investigated by Hayat *et al.* (2016).The numerical method was utilized by Zaimi *et al.* (2013) to investigate visco-elastic fluid flow within a rotating frame that is restricted by a stretchable sheet. The effects of radial stretching in the Von Karman whirling flow issue of an infinite disk were examined by Turkyilmazoglu (2012). Turkyilmazoglu (2014) expanded the Bodewadt flow problem to a disk that is expanding circumferentially and at a constant pace in a radial direction. The aforementioned issue was further upon by Mustafa *et al.* (2015) for the scenario of a nano-fluid containing five different kinds of nanoparticles.

Both homogeneous and heterogeneous reactions occur in the majority of chemical reaction systems. A reaction is said to be homogeneous if it takes place at the same phase in solution while a heterogeneous reaction happens at more than one phase. Many processes containing both reactions are combustion, biochemical system, catalysis, distillation process, hydro-metallurgical devices, production of ceramics, etc. A variety of chemical reactions with practically important applications, proceed very slowly, or not, except in the existence of catalyst. HHR occur at the same time in many chemical systems including catalysis, combustion and biochemical systems. Merkin (1996) used an identical model of HHR in a BLF over a flat surface. His results reveal that heterogeneous (surface) reaction is dominant closer to the leading edge of the surface. Recently, Alam *et al.* (2021) investigated the HHR through a hybrid nano-fluid flowing over a rotating disc. Ahmed *et al.* (2021) studied the physical aspects of HHR on MHD Williamson fluid flow across a non-linear stretching curved sheet. Other researchers also studied on HHR in different fluid flow conditions (Sen *et.al.*, 2021; Reddy *et al.*, 2021)). Recently, some researchers studied the impact of magnetic field in different fluid flow condition (Ali *et al.*, 2022; Ali *et al.*, 2022; Ali et al., 2022; Adem, 2020, 2023)).

The following factors highlight the originality of the current study:

Maqsood *et al.* (2017)studied the viscoelastic FF in rotating frame considering HHR numerically. Motivating from their work we included the magnetic and electric fields on the fluid flow and treated the problem analytically using OHAM. Thus, to the author's knowledge, there are no studies have been communicated so far with regard to the analytical treatment of HHR in electrical MHD non-Newtonian Maxwell fluid flow in a rotating frame. Hence, this article aims to frame the problem of the electrical MHD Maxwell fluid flows and solve analytically using OHAM. Graphical artworks are found and clarified in the presence of new physical characteristics namely non-Newtonian fluid, rotating frame, electric field and HHR in this research.

2. Mathematical Formulation

Assume that an elongated planar elastic surface in the x-direction causes a laminar flow of binary electrically conducting viscoelastic fluid that obeys the Maxwell model. We choose a 3D axis in which $z-axis$ is aligned vertically upward and surface occupies the $xy-plane$. Maxwell fluid filling half space $z>0$ rotates uniformly about $z-axis$ with constant rate Ω (see Fig. 1). The magnetic field B_0 and electric field E_0 are acting in z-direction. We also examine the possibility of species in the flow field that are involved in chemical reactions. Because the flow problem is truly three-dimensional, rotating frame generates a Coriolis force. Hereafter the components of the Coriolis force vector are $\rho(-2\Omega v, 2\Omega u, 0)$. One can suppose that a simple model of HHR occurs, given mathematically by Chaudhary and Merkin (1996) and Maqsood *et al.* (2017)):

$$2B + A \to 3B,\ rate = k_c b^2 a \qquad (1)$$

whereas the catalyst surface is assumed to have an isothermal reaction and to be first-order given by:

$$A \to B,\ rate = a k_s, \qquad (2)$$

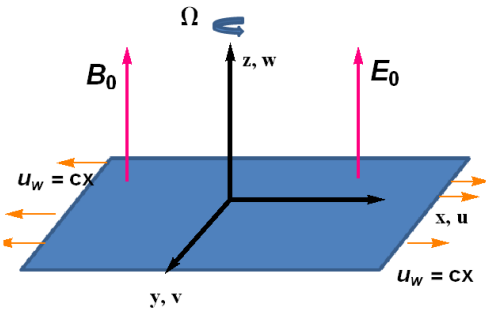

Figure 1. Physical configuration and coordinate system

where a and b symbolize the concentration of chemical species A and B respectively while k_c and$k_s$are constants. The expression (1) confirms that the reaction rate at the outer edge of the BL is zero.

The following are the expressions for the BL equations that describe the flow and MT in a Maxwell fluid. (see, Shah et al. (Shah *et al.*, 2018), Shafique et al. (Shafique, Mustafa and Mushtaq, 2016) and Shah et al.(Shah *et al.*, 2017)):

$$\frac{\partial w}{\partial z} + \frac{\partial v}{\partial y} + \frac{\partial u}{\partial x} = 0, \qquad (3)$$

$$\left(\frac{\partial u}{\partial x}\right)u+\left(\frac{\partial u}{\partial y}\right)v+\left(\frac{\partial u}{\partial z}\right)w-2\Omega v-\nu\frac{\partial^2 u}{\partial z^2}-\ u\frac{\sigma B_0^2}{\rho}+\frac{\sigma B_0 E_0}{\rho}$$
$$+\lambda_1\begin{pmatrix}\left(\frac{\partial^2 u}{\partial x^2}\right)u^2+\left(\frac{\partial^2 u}{\partial y^2}\right)v^2+\left(\frac{\partial^2 u}{\partial z^2}\right)w^2+2uv\frac{\partial^2 u}{\partial x\partial y}+2vw\frac{\partial^2 u}{\partial y\partial z}\\-2\Omega\left(\left(\frac{\partial v}{\partial x}\right)u+\left(\frac{\partial v}{\partial y}\right)v+\left(\frac{\partial v}{\partial z}\right)w\right)+2\Omega\left(v\frac{\partial u}{\partial x}-u\frac{\partial u}{\partial y}\right)+2uw\frac{\partial^2 u}{\partial x\partial z}\end{pmatrix}=0 \quad (4)$$

$$\left(\frac{\partial v}{\partial x}\right)u+\left(\frac{\partial v}{\partial y}\right)v+\left(\frac{\partial v}{\partial z}\right)w+2\Omega u-\nu\frac{\partial^2 v}{\partial z^2}-v\frac{\sigma B_0^2}{\rho}-\frac{\rho B_0 E_0}{\rho}$$
$$+\lambda_1\begin{pmatrix}u^2\left(\frac{\partial^2 v}{\partial x^2}\right)+v^2\left(\frac{\partial^2 v}{\partial y^2}\right)+w^2\left(\frac{\partial^2 v}{\partial z^2}\right)+2uv\frac{\partial^2 v}{\partial x\partial y}+2vw\frac{\partial^2 v}{\partial y\partial z}\\-2\Omega\left(u\frac{\partial u}{\partial x}+v\frac{\partial u}{\partial y}+w\frac{\partial u}{\partial z}\right)+2\Omega\left(v\frac{\partial v}{\partial x}-u\frac{\partial v}{\partial y}\right)+2uw\frac{\partial^2 v}{\partial x\partial z}\end{pmatrix}=0 \quad (5)$$

$$u\frac{\partial a}{\partial x}+v\frac{\partial a}{\partial y}+w\frac{\partial a}{\partial z}=D_A\frac{\partial^2 a}{\partial z^2}-ak_c b^2 \quad (6)$$

$$u\frac{\partial b}{\partial x}+v\frac{\partial b}{\partial y}+w\frac{\partial b}{\partial z}=D_B\frac{\partial^2 b}{\partial z^2}+ak_c b^2 \quad (7)$$

The following are the BCs for the current issue:

$$u_W(x)=u(x,0)=xc,\ \ v(x,0)=0 \quad (8a)$$

$$w(x,0)=0 \quad (8b)$$

$$\begin{cases}D_A\left(\frac{\partial a}{\partial z}\right)_{z=0}=a(x,0)k_s\,,\\ D_B\left(\frac{\partial b}{\partial z}\right)_{z=0}=-a(x,0)k_s\end{cases} \quad (8c)$$

$$u\to 0,\ v\to 0,\ a\to a_0,\ b\to 0,\ \text{as}\ z\to\infty \quad (9)$$

Here u, v and w represent the velocity components in the directions of x, y and z, respectively, λ_1 is the fluid relaxation time, D_A and D_B. D_B stand for respective diffusing coefficients, ν stands for kinematic viscosity and $c>0$ symbolizes the stretching rate. The terms appearing with Ω are as a result of Coriolis force. The last terms in Equations (6) and (7) indicate the consumption rate of chemical species A and production rate of chemical species B, respectively.

It is evident from condition (8a) that there is no requirement for slip at the wall, condition (8b) indicates impermeability of the stretching sheet, conditions (8c) shows that mass fluxes of species A and B are proportional to the concentration of species A at the surface and condition (9) shows that velocity and concentration differences disappear at far distance from the boundary.

By selecting a suitable similarity variable $\eta=z\sqrt{c/\upsilon}$, We suggest the following quantities (see, Bachok et al. (Bachok, Ishak and Pop, 2011) and Maqsood et al.(Maqsood, *et al.*, 2017)):

$$\begin{cases}u=f'(\eta)cx,\ v=r(\eta)cx,\ w=-\sqrt{\upsilon c}f(\eta),\\ a=h(\eta)a_0,\ \ b=H(\eta)a_0,\end{cases} \quad (10)$$

in which prime designates derivative with respect to η. The formulas in Eq. (10) satisfy the continuity Eq. (1) whereas Eqs. (4)– (9) transformed into the BVPs

$$M(E_1-f')-(f')^2-2\lambda(\beta fr'-r)-\beta(f^2f'''-2ff'f'')+f'''+ff''=0, \quad (11)$$

$$r''+fr'-f'r-2\lambda\left(f'+\beta((f')^2-ff''+r^2)\right)+\beta(2ff'r'-f^2r'')-M(r-E_1)=0, \quad (12)$$

$$h''+Sc\left(fh'-K_hhH^2\right)=0, \quad (13)$$

$$\delta H''+Sc(fH'+K_hhH^2)=0, \quad (14)$$

with the BCs given below:

at $\eta = 0$:

$$f = r = 0,\ f' = 1,\ h' = K_s h,\ \delta H' = -K_s h \quad (15)$$

as $\eta \to \infty$:

$$f' \to 0, r \to 0,\ h \to 0,\ H \to 0. \quad (16)$$

The symbols λ, β, Sc, δ, k_h, k_s, M and E_1 represent the rotation-strength parameter, Deborah number, Schmidt number, ratio of diffusion coefficients, homogeneous reaction strength parameter, heterogeneous reaction strength parameter, magnetic and electric field parameters respectively. These are expressed as follows

$$\begin{cases} \beta = \lambda_1 c,\ \lambda = \frac{\Omega}{c},\ Sc = \frac{\nu}{D_A}, K_h = \frac{k_c a_0^2}{c}, \\ M = \frac{\sigma B_0^2}{\rho c}, E_1 = \frac{E_0}{B_0 u_w}, \delta = \frac{D_B}{D_A},\ K_s = \frac{k_s}{D_A}\sqrt{\frac{\nu}{c}}, \end{cases} . \quad (17)$$

The diffusion coefficients of species A and B are expected to be similar in size in many real-world situations. This allows us to assume further that the coefficients D_A and D_B are equal, meaning that $\delta \approx 1$. Considering the circumstances (15) and (16), we can write:

$$h(\eta) + H(\eta) = 1. \quad (18)$$

In light of this, Eqs. (13) and (14) can be combined to get the single equation that follows:

$$h'' + Sc\left(fh' - K_h h(1-h)^2\right) = 0 \quad (19)$$

subjected to the BCs:

$$h'(0) = K_s h(0) \text{ and } h(\infty) \to 1. \quad (20)$$

Skin friction coefficients along the x- and y-directions are defined as follows:

$$C_{fx} = \frac{\tau_{wx}}{\rho u_w^2}, C_{fy} = \frac{\tau_{wy}}{\rho v_w^2},$$

where the surface shear stresses τ_{wx} and τ_{wy} along the x-and y - directions are given by

$$\tau_{wx} = \mu\left[\frac{\partial u}{\partial z}\right]_{z=0}, \tau_{wy} = \mu\left[\frac{\partial v}{\partial z}\right]_{z=0}.$$

Dimensionless skin friction coefficients are

$$C_{fx}(Re_x)^{\frac{1}{2}} = (1+\beta)f''(0), C_{fy}(Re_y)^{\frac{1}{2}} = (1+\beta)r'(0)$$

Where $(Re_x)^{\frac{1}{2}} = x\sqrt{c/\upsilon}, (Re_y)^{\frac{1}{2}} = y\sqrt{c/\upsilon}$ denote the local Reynolds number.

3. Analytical Solution Using OHAM

The OHAM is now applied to non-linear ODEs (11), (12) and (19) along with the BCs (15) and (16) by considering the following assumptions

$$\begin{cases} g = g_0 + pg_1 + p^2 g_2, f = f_0 + pf_1 + p^2 f_2, \\ h = h_0 + ph_1 + p^2 h_2, H_1(p) = pC_1 + p^2 C_2, \\ H_2(p) = pC_3 + p^2 C_4, H_3(p) = pC_5 + p^2 C_6, \end{cases} \quad (21)$$

where $p \in [0,1]$ represented an embeding parameter, $H_j(p)$, $j = 1,2,3$ is an auxiliary function different from zero, and C_i, $(i = 1,2,3,4,5,6)$ are convergence parameters (Marinca *et al.* (Marinca *et al.*, 2009)).

3.1. Analytical Solution of the Momentum BLP in the $x-axis$

The following supposition is used when applying the OHAM to Eq. (11):

$$L = f''' + f'$$ and

$$N = f''' + ff'' - (f')^2 - 2\lambda(\beta f r' - r) - \beta(f^2 f''' - 2ff'f'') + M(E_1 - f') - (f'' + f'), \quad (22)$$

Where L and N are the linear and non-linear operators, respectively. Consequently, the equation of OHAM family is written as follows.

$$(1-p)(f''+f') = H_1(p)\begin{bmatrix} f'''+ff''-(f')^2-2\lambda(\beta fr'-r) \\ -\beta(f^2f'''-2ff'f'')+M(E_1-f') \end{bmatrix}. \quad (23)$$

Following a lengthy exercise, utilizing the BCs (15-16) and equating the same powers of $p-terms$, we have got the following:

When we solve the zero-order equation p^0, we got

$$f_0'+f_0''=0, \quad f_0(0)=0, \quad f_0'(0)=1. \quad (24)$$

$$f_2''+f_2'=f_1'+f_1''+C_1\begin{bmatrix} f_1f_0''-2f_0'f_1'-Mf_1'-2(-\lambda r_1+\lambda\beta(f_0r_1'+f_1r_0')) \\ ME_1-\beta\left[f_1^2f_0'''-2\begin{pmatrix} f_0f_1'f_1''-f_0f_1f_1''' \\ +f_1f_0'f_1''+f_1f_1'f_0'' \end{pmatrix}\right]+f_0f_1''+f_1''' \end{bmatrix}$$
$$+C_2\begin{bmatrix} f_0'''-f_0'^2+f_0f_0''-2(\beta\lambda f_0r_0'-\lambda r_0) \\ -\beta(f_0^2f_0'''-2f_0f_0'f_0'')-M(E_1-f_0') \end{bmatrix}, \quad (25)$$

$$f_2(0)=0, \; f_2'(0)=0. \quad (26)$$

The following was the result of solving ODEs (24)–(26) with the associated BCs:

$$f_0=1-e^{-\eta} \quad (27)$$

$$f_1=\frac{C_1e^{-3\eta}}{6}\begin{pmatrix} 6M(e^{2\eta}-e^{3\eta})-6e^{\eta}\beta\eta\lambda+ \\ 6e^{2\eta}E_1M-6e^{3\eta}E_1M+\beta+ \\ 3e^{2\eta}\beta-4e^{3\eta}\beta+6e^{2\eta}M\eta+ \\ 6e^{3\eta}E_1M\eta+6e^{2\eta}\beta\eta-12e^{2\eta}\lambda+ \\ 12e^{3\eta}\lambda-3e^{\eta}\beta\lambda+3e^{3\eta}\beta\lambda \\ -12e^{2\eta}\eta\lambda-6e^{2\eta}\eta^2\lambda-6e^{2\eta}\beta\eta^2\lambda \end{pmatrix} \quad (28)$$

The size of the term, f_2, prevents its mention here. Thus, the answer $f(\eta)$ is stated as:

$$f(\eta,C_i)=f_0(\eta,C_i)+f_1(\eta,C_i)+f_2(\eta,C_i), \text{ where } i=1,2,3,4. \quad (29)$$

Utilizing the equation of residual for the issue revealed in the form, we can determine the unknown constants.

$$R_1(\eta,C_i)=f'''+ff''-(f')^2-2\lambda(\beta fr'-r)-\beta(f^2f'''-2ff'f'')+M(E_1-f'). \quad (30)$$

The next conditions, which are listed below, can best be used to get the parameters of convergence C_i, $i=1,2,3,4$.

$$\frac{\partial J_1(C_i)}{\partial C_1}=\frac{\partial J_1(C_i)}{\partial C_2}=\frac{\partial J_1(C_i)}{\partial C_3}=\frac{\partial J_1(C_i)}{\partial C_4}=0, \text{ where } J_1(C_i)=\int_0^5 R_1^2(\eta,C_i)d\eta. \quad (31)$$

Consequently, the condensed solution will be

$$f(\eta)=f_0(\eta)+f_1(\eta)+f_2(\eta) \quad (32)$$

The parameters of convergence are computed using $\beta=0, E_1=0.1, M=0.2,$ and $\lambda=0.3,$ is a specific instance.

$C_1=0.8176030448003411,$
$C_2=0.5245380836764166,$
$C_3=0.5144612280520182,$
$C_4=0.05601353192963746.$

The semi-analytical solution can be presented as:

$$f(\eta)=1-e^{-\eta}+0.1362671741e^{-3\eta}\begin{pmatrix} 0.-2.27999999994e^{2\eta}+2.2799999999994e^{3\eta} \\ -2.3999999999995e^{2\eta}\eta+0.1200000000002e^{3\eta}\eta \\ -1.799999999998e^{2\eta}\eta^2 \end{pmatrix}+f_2(\eta,C_i). \quad (33)$$

When the parameters are substituted, we obtain

$$f(\eta) = 1 - e^{-\eta} + 0.1362671741e^{-3\eta}\begin{pmatrix} 0. - 2.279999999994e^{2\eta} + 2.2799999999994e^{3\eta} \\ -2.3999999999995e^{2\eta}\eta + 0.1200000000002e^{3\eta}\eta \\ -1.799999999998e^{2\eta}\eta^2 \end{pmatrix} + \frac{e^{-5\eta}}{21600}\begin{pmatrix} -1514.25023935338e^{2\eta} - 1607.3394846448e^{3\eta} \\ +8380.22046829731e^{4\eta} - 5258.630744299022e^{5\eta} \\ +505.216346032604e^{4\eta}\eta + 117.574434914767e^{5\eta}\eta \\ -4305.93219299421e^{4\eta}\eta^2 + 242.280038296542e^{4\eta}\eta^3 \end{pmatrix} \quad (34)$$

3.2. Analytical Solution of the Momentum BLP in the $y-axis$

Non-linear ODE (12) is subjected to the OHAM by applying the following assertion.

$L = r + r'$ and

$$N = r'' + fr' - f'r - 2\lambda(f' + \beta(f')^2 - (ff'' + r^2) + fr' + \beta\left(2ff'r' - f^2r''\right) - M(r - E_1) - \left(r' + r\right), \quad (35)$$

where L and N are the linear and non-linear operators, respectively. The OHAM family equation is thus written as:

$$(1-p)\left(r' + r\right) = H_2(p)\begin{pmatrix} r'' - f'r - 2\lambda\left(f' + \beta\left((f')^2 - ff'' + r^2\right)\right) \\ +\beta\left(2ff'r' - f^2r''\right) - M(r - E_1) + fr' \end{pmatrix}. \quad (36)$$

Following simplification, utilizing the BCs (15-16), equating the similar powers of $p-terms$, we arrive at the following:

When we solve the zero-order equation p^0, we get:

$$r_0' + r_0 = 0, \quad r_0(0) = 0 \quad (37)$$

When we solve the first-order equation p^1, we get

$$r_1' + r_1 = r_0' + r_0 + C_3\begin{bmatrix} -M(r_0 - E_1) + 2\lambda\left(f_0' + \beta\left(f_0'^2 - f_0f_0'' + r_0^2\right)\right) \\ +\beta\left(2f_0f_0'r_0' - r_0''f_0^2\right)r_0'' - f_0'r_0 + f_0r_0' \end{bmatrix}, \; r_1(0) = 0. \quad (38)$$

When we solve the second-order equation p^2, we get

$$r_2' + r = r_1' + r_1 + C_3\begin{pmatrix} f_1r_0' - f_0'r_1 - f_1'r_0 - 2\lambda\left(f_1' + \beta\begin{pmatrix} 2f_0'f_1' - f_0f_1'' \\ -f_1f_0'' + 2r_0r_1 \end{pmatrix}\right) \\ + \beta\begin{pmatrix} 2\begin{pmatrix} f_0f_1'r_1' + f_1f_0'r_1' \\ +f_1f_1'r_0' \end{pmatrix} \\ -2r_0r_1r_1'' - r_1^2r_0'' \end{pmatrix} - M(r_1 - E_1) + r_1'' + f_0r_1' \end{pmatrix}$$

$$+C_4\begin{bmatrix} f_0r_0' + 2\lambda\left(f_0' + \beta\left(f_0'^2 - f_0f_0'' + r_0^2\right)\right) + \\ \beta\left(2f_0f_0'r_0' - r_0''f_0^2\right) - M(r_0 - E_1) + r_0'' - f_0'r_0 \end{bmatrix}, \quad r_2(0) = 0. \quad (39)$$

When the ODEs (37) through (39) are solved using the associated BCs, we obtain

$$r_0 = \eta e^{-\eta} \quad (40)$$

$$r_1 = -\frac{e^{-3\eta}}{4}\begin{pmatrix} -4\,C_3\,e^{\eta} + 4\,C_3\,e^{2\eta} + 4\,C_3\,e^{2\eta}\,E_1\,M - 4C_3\,e^{3\eta}E_1\,M \\ +C_3\,\beta - 8C_3\,e^{\eta}\,\beta + 7\,C_3\,e^{2\eta}\,\beta - 4\,e^{2\eta}\,\eta + 4C_3\,e^{2\eta}\,\eta \\ +2\,C_3\,\beta\,\eta - 8C_3\,e^{2\eta}\beta\,\eta + 2\,C_3\,e^{2\eta}\,M\,\eta^2 + 2\,C_3\,e^{2\eta}\,\beta\,\eta^2 \\ -16C_3\,e^{\eta}\,\beta\,\lambda + 16C_3\,e^{2\eta}\,\beta\,\lambda + 8\,C_3\,e^{2\eta}\,\eta\,\lambda - 16C_3\,e^{\eta}\,\beta\,\eta\,\lambda \\ +8\,C_3\,e^{2\eta}\,\beta\,\eta\,\lambda - 8\,C_3\,e^{\eta}\beta\,\eta^2\,\lambda \end{pmatrix} \quad (41)$$

The size of the other term, r_2, prevents its mention here. Thus, the answer $r(\eta)$ is stated as:

$$r(\eta, C_i) = r_0(\eta, C_i) + r_1(\eta, C_i) + r_2(\eta, C_i),\ i = 1,2,3,4. \quad (42)$$

The problem's residual equation, which takes the form:

$$R_2(\eta, C_i) = r'' + fr' - f'r - 2\lambda\left(f' + \beta((f')^2 - ff'' + r^2)\right) + \beta(2ff'r' - f^2r'') - M(r - E_1). \quad (43)$$

The next conditions can be used to determine the parameters $C_i,\ i = 1,2,3,4.$

$$\frac{\partial J_2(C_i)}{\partial C_1} = \frac{\partial J_2(C_i)}{\partial C_2} = \frac{\partial J_2(C_i)}{\partial C_3} = \frac{\partial J_2(C_i)}{\partial C_4} = 0, \text{ where } J_2(C_i) = \int_0^5 R_2^2(\eta, C_i)d\eta. \quad (44)$$

Once the parameters have been obtained, the solution will be provided by

$$r(\eta) = r_0(\eta) + r(\eta) + r_2(\eta). \quad (45)$$

In specific circumstances, $\beta = 0$, $E_1 = 0.1$, $M = 0.2$, and $\lambda = 0.3$, the convergence parameter values are calculated as

$$C_1 = 0.8176030448003411,$$
$$C_2 = 0.5245380836764166,$$
$$C_3 = 0.5144612280520182,$$
$$C_4 = 0.05601353192963746.$$

The approximate semi-analytical solution is expressed as

$$r(\eta, C_i) = \eta e^{-\eta} - \frac{e^{-3\eta}}{4}\begin{pmatrix} -4\,C_3\,(e^{\eta} - e^{2\eta} + 4\,e^{\eta}\,\beta\,\eta\,\lambda) - 4\,C_3\,e^{2\eta}\,E_1\,M + 4C_3\,e^{3\eta}E_1\,M \\ +C_3\,\beta - 8C_3\,e^{\eta}\,\beta + 7\,C_3\,e^{2\eta}\,\beta - 4\,e^{2\eta}\,\eta + 4C_3\,e^{2\eta}\,\eta + 2\,C_3\,\beta\,\eta \\ -8C_3\,e^{2\eta}\beta\,\eta + 2\,C_3\,e^{2\eta}\,M\,\eta^2 + 2\,C_3\,e^{2\eta}\,\beta\,\eta^2 - 16C_3\,e^{\eta}\,\beta\,\lambda \\ +16C_3\,e^{2\eta}\,\beta\,\lambda + 8\,C_3\,e^{2\eta}\,\eta\,\lambda + 8\,C_3\,e^{2\eta}\,\beta\,\eta\,\lambda - 8\,C_3\,e^{\eta}\beta\,\eta^2\,\lambda \end{pmatrix} + r_2(\eta, C_i). \quad (46)$$

After changing the parameters, we obtained

$$r(\eta) = e^{-\eta}\eta - \frac{e^{-3\eta}}{4}\begin{pmatrix} -2.057844912208073e^{\eta} + 2.016688013963911e^{2\eta} \\ +0.0411568982441614e^{3\eta} - 0.70744814046708e^{2\eta}\eta \\ +0.20578449122080e^{2\eta}\eta^2 \end{pmatrix}$$
$$+\frac{e^{-5\eta}}{864}\begin{pmatrix} -114.337593432917e^{2\eta} + 34.20160830622876e^{3\eta} \\ +93.44012892104615e^{4\eta} - 13.304143794357435e^{5\eta} \\ -263.7870718400552e^{3\eta}\eta + 142.8809552579719e^{4\eta}\eta \\ -109.026017233444e^{3\eta}\eta^2 - 81.5275282488180e^{4\eta}\eta^2 \\ -22.703502583882e^{4\eta}\eta^3 \end{pmatrix} \quad (47)$$

3.3. Analytical Solution of the Concentration BLPs

The OHAM is employed to Equation (19) under the next statements

$$L = h' + h \text{ and}$$

$$N = h'' + Sc\left(fh' - K_h h(1-h)^2\right) - \left(h' + h\right), \quad (48)$$

where L and N are the linear and non-linear operators, respectively. The OHAM family of equations is thus given by

$$(1-p)\left(h' + h\right) = H_3(p)\left[h'' + Sc\left(fh' - K_h h(1-h)^2\right)\right] \quad (49)$$

The following results are obtained after simplifying, equating similar powers of $p-terms$, and applying BCs (15-16):

When we solve the zero-order equation p^0, we get

$$h_0' + h = 0, \;\; h_0'(0) = K_s h_0(0). \quad (50)$$

When we solve the 1st-order equation p^1, we get

$$h_1' + h_1 = h_0' + h_0 + C_5\left[h_0'' + Sc\left(f_0 h_0' - K_h h_0(1-h_0)^2\right)\right], \; h_1'(0) = 0. \quad (51)$$

When we solve the 2nd -order equation p^2, we get

$$h_2' + h_2 = h_1' + h_1 h_2' + h_2 = h_1' + h_1 + C_5\left[h_1'' + Sc\left(f_0 h'_1 + f_1 h_0' - K_h h_1(1-h_1)^2\right)\right]$$
$$+C_6\left[h_0'' + Sc\left(f_0 h_0' - K_h h_0(1-h_0)^2\right)\right], \;\; h_2'(0) = 0. \quad (52)$$

On solving the ODEs (50)-(52), with the BCs, we obtained:

$$h_0 = \frac{e^{-\eta}\left(e^{\eta} - K_s + e^{\eta}K_s\right)}{1+K_s} \quad (53)$$

$$h_1 = \frac{e^{-3\eta}}{2(1+K_s)^3}\begin{pmatrix} 2e^{3\eta} - 2C_5e^{2\eta}K_s + 6e^{3\eta}K_s - 4C_5e^{2\eta}{K_s}^2 + 6e^{3\eta}{K_s}^2 - 2C_5e^{2\eta}{K_s}^3 \\ +2e^{3\eta}{K_s}^3 + 2C_5e^{\eta}K_s\mathrm{Sc} - C_5K_hK_s{}^3\mathrm{Sc} + 2C_5e^{\eta}K_hK_s{}^3\mathrm{Sc} - C_5e^{2\eta}K_hK_s{}^3\mathrm{Sc} \\ -2C_5e^{2\eta}K_s\eta - 4C_5e^{2\eta}{K_s}^2\eta - 2C_5e^{2\eta}{K_s}^3\eta + 2C_5e^{2\eta}K_s\mathrm{Sc}\eta - 2C_5e^{2\eta}K_s{}^3\mathrm{Sc} \\ +4C_5e^{2\eta}{K_s}^2\mathrm{Sc}\eta + 2C_5e^{2\eta}K_s{}^3\mathrm{Sc}\eta - 2C_5e^{2\eta}K_s\mathrm{Sc} + 4C_5e^{\eta}{K_s}^2\mathrm{Sc} \\ -4C_5e^{2\eta}{K_s}^2\mathrm{Sc} + 2C_5e^{\eta}K_h{K_s}^2\mathrm{Sc} - 4C_5e^{2\eta}K_h{K_s}^2\mathrm{Sc} + 2C_5e^{\eta}K_s{}^3\mathrm{Sc} \end{pmatrix} \quad (54)$$

The size of the other term, h_2, prevents its mention here. Thus, the expression of the solution is written as:

$$h(\eta, C_i) = h_0(\eta, C_i) + \ h_1(\eta, C_i) + \ h_2(\eta, C_i), \ i = 1,2,3,4,5,6. \quad (55)$$

The problem's residual equation, which takes the form:

$$R_3(\eta, C_i) = h^{''} + Sc\left(fh^{'} - K_h h(1-h)^2\right). \quad (56)$$

The following circumstances lead to the best identification of the parameters C_i :

$$\frac{\partial J_3(C_i)}{\partial C_1} = \frac{\partial J_3(C_i)}{\partial C_2} = \frac{\partial J_3(C_i)}{\partial C_3} = \frac{\partial J_3(C_i)}{\partial C_4} = \frac{\partial J_3(C_i)}{\partial C_5} = \frac{\partial J_3(C_i)}{\partial C_6} = 0, \quad (57)$$

$$\text{where } J_3(C_i) = \int_0^5 R_3^2\,(\eta, C_i)d\eta.$$

Once the parameters have been obtained, the simplified solution will be provided by

$$h(\eta) = h_0(\eta) + \ h_1(\eta) + \ h_2(\eta). \quad (58)$$

Considering particular cases, when $\beta = 0, E_1 = 0.1,\ M = 0.2,$ and $\lambda = 0.3,$ The parameters are calculated and given below

$$C_1 = 0.8176030448003411,\ C_2 = 0.5245380836764166,\ C_3 = 0.5144612280520182,$$
$$C_4 = 0.05601353192963746,\ C_5 = -0.6655321550273889,\ C_6 = 9.210023457455835.$$

Hence the analytical solution is given by:

$$h(\eta, C_i) = \frac{e^{-\eta}(\,e^{\eta} - K_s + \ e^{\eta}K_s)}{1+K_s} + \frac{e^{-3\eta}}{2(1+K_s)^3}\begin{pmatrix} 2e^{3\eta} - 2C_5e^{2\eta}K_s + 6e^{3\eta}K_s - 4C_5e^{2\eta}{K_s}^2 + \\ 6e^{3\eta}{K_s}^2 - 2C_5e^{2\eta}{K_s}^3 + 2e^{3\eta}{K_s}^3 + 2C_5e^{\eta}K_s\mathrm{Sc} - \\ C_5K_hK_s{}^3\mathrm{Sc} + 2C_5e^{\eta}K_hK_s{}^3\mathrm{Sc} - C_5e^{2\eta}K_hK_s{}^3\mathrm{Sc} - \\ 2C_5e^{2\eta}K_s\eta - 4C_5e^{2\eta}{K_s}^2\eta - 2C_5e^{2\eta}K_s{}^3\eta + \\ 2C_5e^{2\eta}K_s\mathrm{Sc}\eta + 4C_5e^{2\eta}{K_s}^2\mathrm{Sc}\eta + 2C_5e^{2\eta}K_s{}^3\mathrm{Sc}\eta - \\ 2C_5e^{2\eta}K_s\mathrm{Sc} + 4C_5e^{\eta}{K_s}^2\mathrm{Sc} - 4C_5e^{2\eta}{K_s}^2\mathrm{Sc} + \\ 2C_5e^{\eta}K_h{K_s}^2\mathrm{Sc} - 4C_5e^{2\eta}K_h{K_s}^2\mathrm{Sc} + 2C_5e^{\eta}K_s{}^3\mathrm{Sc} - \\ 2C_5e^{2\eta}K_s{}^3\mathrm{Sc} \end{pmatrix} + \ h_2(\eta, C_i) \quad (59)$$

Upon changing the parameters, we have obtained:

$$h(\eta) = 0.666666666666e^{-\eta}(-0.5 + 1.5e^{\eta}) + 0.1481481481481e^{-3\eta}\begin{pmatrix}0.0831915193 + 6.75e^{3\eta} - 3.494043813893792e^{\eta} \\ +5.24106572084068e^{2\eta} - 1.4974473488116e^{2\eta}\eta\end{pmatrix} + 0.0018289894e^{-5\eta}\begin{pmatrix}-0.37372476041049413 + 30.894580193934182e^{\eta} \\ -559.6485211167734e^{2\eta} + 3938.1560196506844e^{3\eta} \\ -5197.4129782e^{4\eta} + 546.7e^{5\eta} + 13.454091374777787e^{2\eta}\eta \\ -413.60489891073127e^{3\eta}\eta + 1521.814002203007e^{4\eta}\eta \\ -59.501831074285946e^{3\eta}\eta^2 - 42.34566849347625e^{4\eta}\eta^2\end{pmatrix} \quad (60)$$

4. Results and Discussion

A linearly deforming surface limits the rotational flow of electrical MHD Maxwell fluid, and a model is created for its effects. The group of nonlinear ODEs (11), (12) and (19) subject to the BCs (15) and (16) is solved analytically by using the OHAM. We make known the results to keep up the effect of various parameters such as electric field, Deborah number, rotation strength parameter, HHT strength parameters on the velocity and concentration curves. We conducted a comparison for $f''(0)$ with the results from other studies, as shown in Table 1, to verify the validity of the OHAM employed in this investigation. The current limiting results are thought to fit up well with the findings of earlier articles that have been published. Table 2 demonstrates that as the magnetic field parameter increases, skin friction also rises. The skin friction does, however, decrease as the electric field parameter increases.

Figs. 2- 4 illustrate how velocity profiles are impacted by the magnetic field M in both the absence and presence of an electric field. Figures 2 depicts the impact on the velocity curve $f'(\eta)$ in the nonappearance of an electric field. The velocity curve is significantly diminished as the value of M is raised. Because there is no electric field, the Lorenz force upsurges the frictional force, functioning as a decelerating force that opposes the Maxwell fluid flow. The fluid's velocity decreases when an electric field is present $\left(E_1 \neq 0\right)$ in the direction that M rises, as seen in Fig.3. It greatly outperforms the stretched sheet after it reaches a certain distance from the wall. An electric field that also accelerates the body force upsurges the Maxwell fluid flow. Figure 4 illustrates how, as M increases, the velocity curve $r(\eta)$ in the y -direction rises. This results from the effect of the Coriolis force on the Maxwell fluid's velocity in the y -direction.

Table 1. Comparison of $f''(0)$ with previous results for different values of λ when $E_1 = M = \beta = 0$

λ	Zaimi et al. (Zaimi, Ishak and Pop, 2013)	Maqsood et al. (Maqsood, Khan and M.Mustafa, 2017)	Present
0.0	-1.0000	-1.000000	-1.000000
0.2	-1.0331	-1.033105	-1.033994
0.4	-1.1009	-1.100905	-1.105931
0.5	-1.1384	-1.138381	-1.137199
0.6	-1.1764	-1.176365	-1.179597
0.8	-1.2581	-1.251776	-1.220244
1.0	-1.3250	-1.325029	-1.354025

Table 2. Values of the skin-friction $C_{fx}(Re_x)^{\frac{1}{2}}$ for dissimilar values of λ, $E_1$and M when $\beta = 0.4$

λ	E_1	M	$C_{fx}(Re_x)^{\frac{1}{2}}$
0.1	0.1	0.2	− 1.167806
0.3	0.1	0.2	− 1.215860
0.5	0.1	0.2	− 1.293328
0.1	0.3	0.2	− 1.115144
0.1	0.5	0.2	− 1.065529
0.1	0.8	0.2	− 0.995009
0.1	0.1	0.4	−0.967055
0.1	0.1	0.6	−1.224972
0.1	0.1	0.8	−1.270143

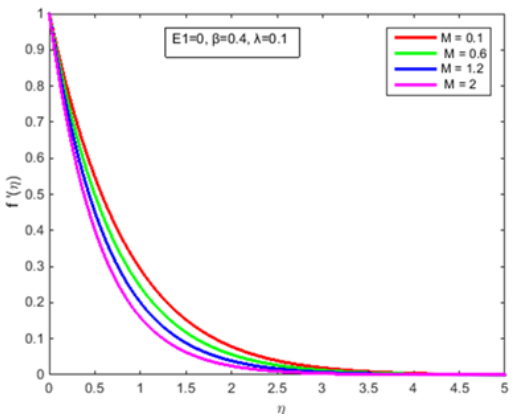

Figure 2. Curves of velocity f'(η) for various values of M in the absence of electric field E_1

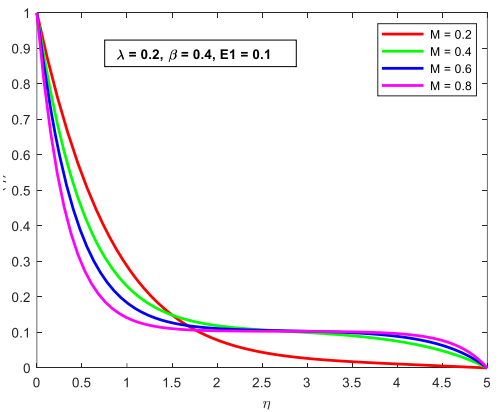

Figure 3. Curves of velocity f'(η) for various values of Min the presence of electric field E_1

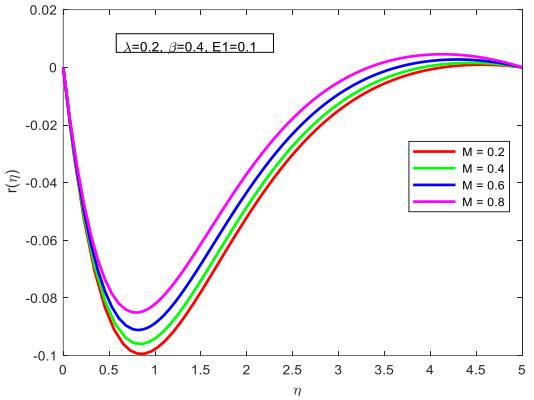

Figure 4. Curves of velocity f'(η) for various values of M

The impact of E_1on the velocity curves are displayed in Figs. 5 and 6. As can be observed, the velocity along the $x-$ direction and y -direction profiles upsurge as the value of the electric field increases. This is because the stronger Lorentz force produced by the electric field accelerates the streamlines away from the stretched plate by reducing frictional resistance. The Maxwell fluids' velocity increases in both directions as a result.

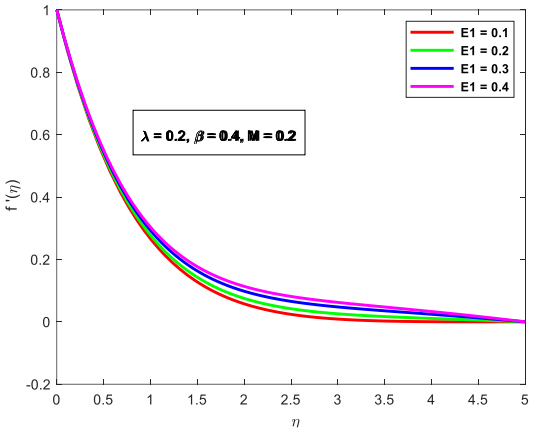

Figure 5. Curves of velocity f'(η) for various values of electric field parameter E_1

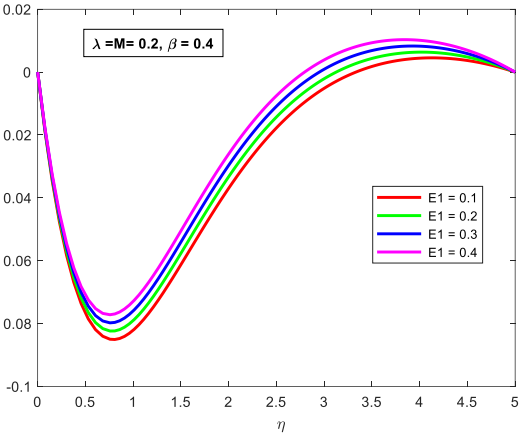

Figure 6. Curves of velocity $r(\eta)$ for various values of electric field parameters E_1.

Velocity curves f'(η) and r(η) for different values of Deborah number β are illustrated for a given rotation-strength parameterλin Figs. 9 and 10, respectively. The curves f'(η) and r(η) are exponentially decrease to zero at closer distances from the sheet as β increases. This illustrates how the depth of momentum penetration decreases as the elastic effect increases. Higher Deborah numbers correspond more closely to the fluid behavior a slower rate of recovery. As a result, as β rises, fluid flow slows in both the x and y -directions and the boundary layer thins. Moreover, the function $r(\eta)$ exhibits a mixed behavior for the parameter β. The change in concentration $h(\eta)$ as the rotation-strength parameter λ is adjusted is shown in Fig.1.

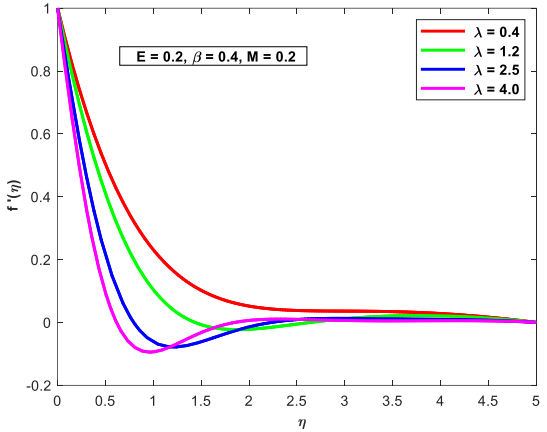

Figure 7. Curves of velocity$f'(\eta)$ for different values of rotation strength parameter λ

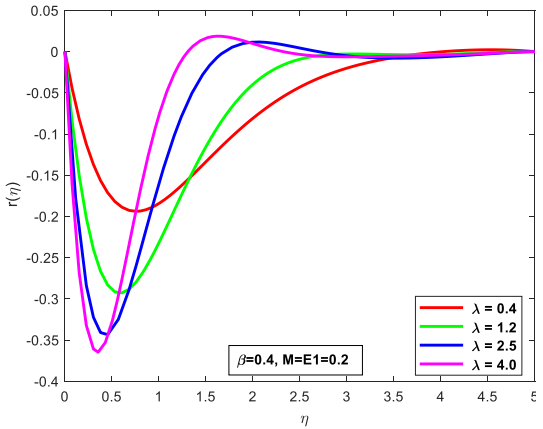

Figure 8. Curves of velocity $r(\eta)$ for different values of rotation strength parameter λ.

As $\eta \to \infty$, we observed that the concentration curve $h(\eta)$ asymptotically approaches 1 and has a finite value at the wall. When the fluid is rotated at a higher pace, one can see that $h(\eta)$ decreases and the concentration layer expands. The fluctuation in concentration profile $h(\eta)$ when the Deborah number β is adjusted is shown in Fig. 12. Concentration decreases as β increases, but its profile widens to indicate an increase in the thickness of the concentration layer.

The variation in the concentration profile $h(\eta)$ as the Schmidt number Sc varies is shown in Fig. 13. For higher values of Sc, a rising trend in $h(\eta)$ is shown. Nevertheless, as Sc increases, the concentration BL strength parameter, K_h , on the concentration curve $h(\eta)$ is portrayed in Fig. 4. As the homogenous reaction gets stronger, the concentration decreases and the concentration BL thickens. The evolution of concentration profiles for different values of the heterogeneous (surface) reaction strength parameter K_s is depicted in Fig. 15.decreases. Physically, a larger value of Sc implies a lesser mass diffusion coefficient, which leads to a shorter concentration BL. The behavior of the homogeneous reaction The concentration curve becomes less steep as the heterogeneous reaction intensity increases. It can be inferred from the fact that when K_h or K_s increase, reactants are consumed in the flow field, causing $h(\eta)$ to decrease. For different values of K_s, Fig. 16 displays the profiles of surface concentration $h(0)$ against parameter K_h. It is evident that when K_s increases, the concentration at the surface drops. It's interesting to note that for all used values of K_s, $h(0)$ varies linearly with K_h . Fig. 17 shows the variation in surface concentration $h(0)$ with Schmidt number Sc for different values of K_s. The surface concentration $h(0)$ expands nonlinearly with an increase in Schmidt number Sc, and this growth becomes more pronounced when larger values of K_s are taken into consideration.

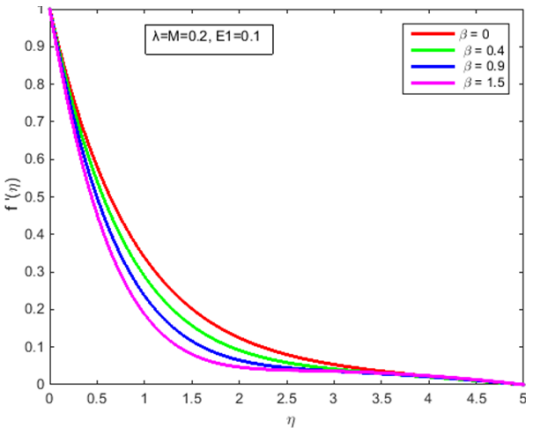

Figure 9. Curves of velocity f'(η) for different values of Deborah number β

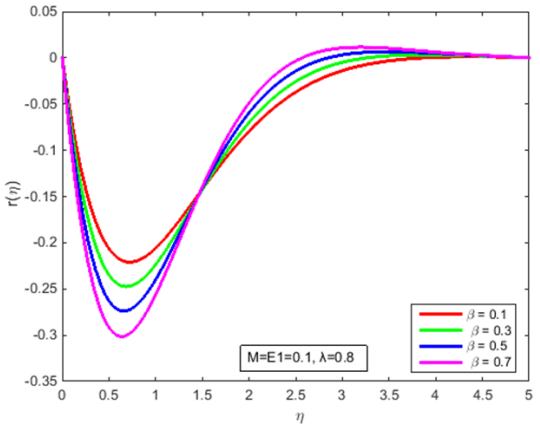

Figure 10. Curves of velocity r(η) for different values of Deborah number β

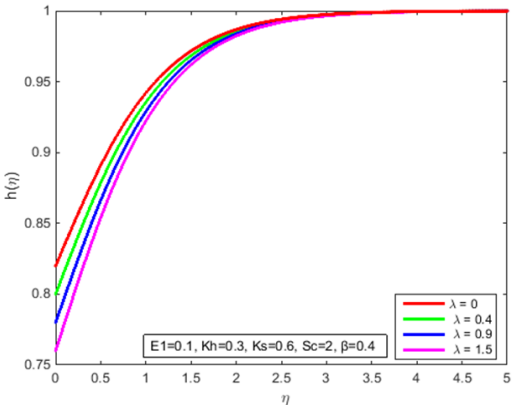

Figure 11. Curves of concentration h(η) for different values of rotation strength parameter λ

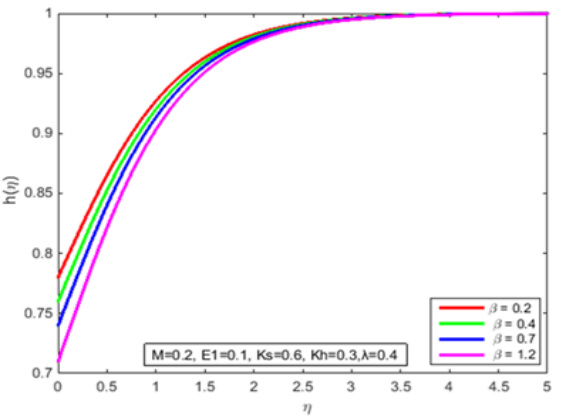

Figure 12. Curves of concentration h(η) for different values of Deborah number β

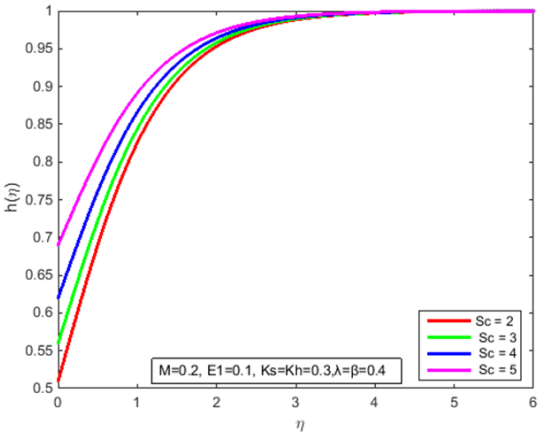

Figure 13. Curves of concentrationh(η) for different values of *Sc*

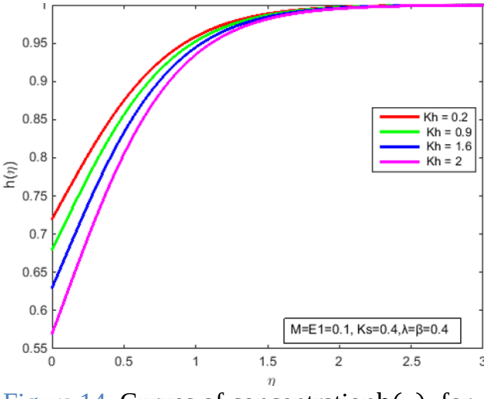

Figure 14. Curves of concentrationh(η) for different values of K_h

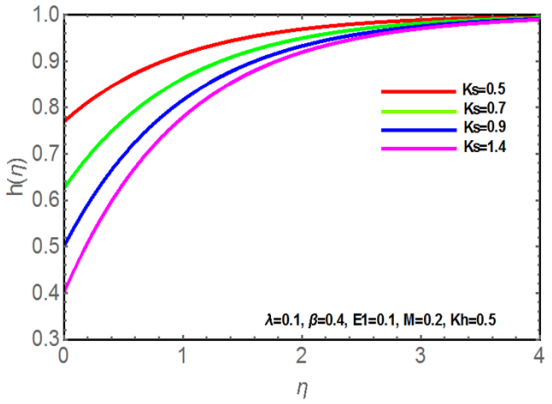

Figure 15. Curves of concentration h(η) for different values of K_s

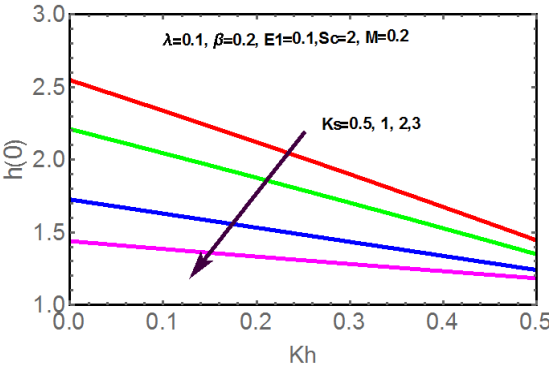

Figure 16. Profiles of surface concentration h(0) for different values of K_s against K_h

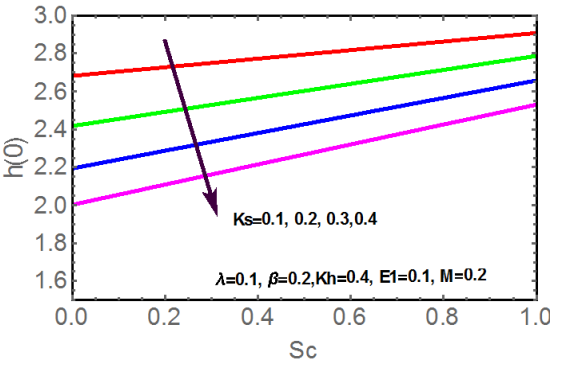

Figure 17. Profiles of surface concentration h(0) for different values of K_s against the Schmidt number Sc

Conclusions

To understand the rotating flow of electrical MHD Maxwell fluid over a stretching sheet, the HHR model is explored. On the BLF of electrical MHD Maxwell fluid across a stretched surface, we have examined the effects of an electric field, a magnetic field, the Deborah number, and the Rotation strength parameter. The controlling PDEs were converted into the dimensionless ODEs by use of similarity transformations. We have used OHAM to analytically solve the transformed equations. In-depth arguments are made for the graphical representations of our findings on the impact of important parameters on the concentration and velocity profiles. Following are a few of the specific conclusions that may be drawn from the study.

- The semi-analytic method OHAM is very effective, simple, fast convergent and is independent of the assumption of the unrealistic small parameters.
- Using the convergence parameters, the series solution may be easily controlled and modified.
- The velocity of fluid flow is increased by an electric field with a higher value. electric field with a higher value.
- Increasing M declines the velocity field

initially and after some time it becomes increasing significantly in the presence of electric field.

- The rotation-strength parameter λ has a delaying impact on the velocity profiles. Also, concentration BL expands when fluid is exposed to a higher rotation rate.
- With growth in fluid relaxation time, BL becomes thinner while an expansion in concentration BL is portrayed.
- Concentration profile declines with growing strengths of HHR.
- From the graphs of $r(\eta)$ againstη, one can observe that counter-clockwise rotation sets up the fluid flow only in the negative y-direction.
- Surface concentration $h(0)$ rises non-linearly for the growing values of Schmidt numberSc.

Abbreviations

BC : Boundary Condition
BL : Boundary layer
BLF: Boundary layer flow
BLP: Boundary layer problem
BLT: Boundary layer thickness
FF : Fluid Flow
HT : Heat Transfer
HHR : Homogeneous-heterogeneous reaction
MHD : Magneto-hydrodynamic
MT : Mass Transfer
ODE : Ordinary differential equation
OHAM : Optimal homotopy asymptotic method
PDE : Partial differential equation

Availability of Data and Materials

Data sharing is not applicable because no datasets were created for the research in this paper.

Competing Interest

The author declared that there were no potential conflicts of interest with regard to the research, authorship, and/or publication of this work.

References

Ahmed, K., Akbar, T. and Muhammad, T. (2021). Physical Aspects of Homogeneous-Heterogeneous Reactions on MHD Williamson Fluid Flow across a Nonlinear Stretching Curved Surface Together with Convective Boundary Conditions', *Mathematical Problems in Engineering*, 1–13. Available at: https://doi.org/https://doi.org/10.1155/2021/7016961.

Alam, M.W., Hussain, S.G., Souayeh, B., Khan, M.S., and Farhan, M. (2021). Numerical Simulation of Homogeneous–Heterogeneous Reactions through a Hybrid Nanofluid Flowing over a Rotating Disc for Solar Heating Applications', *Sustainability*, 13(15): 8289 at: https://doi.org/10.3390/su13158289.

Ali, L., Ali, B., Liu, X., Iqbal, T., Zulqarnain, R.M. and Javid, M. (2018). Three-dimensional magnetohydrodynamic (MHD) flow of Maxwell nanofluid containing gyrotactic micro-organisms with heat source/sink. *AIP Advances 8, 085303* [Preprint]. Available at: https: //doi.org/ 10.1063/ 1.5040540.

Ali, L., Ali, B., Liu. X. , Ahmed, S., Shah, M.A. (2022). A comparative study of unsteady MHD Falkner–Skan wedge flow for non-Newtonian nanofluids considering thermal radiation and activation energy. *Chinese Journal of Physics*, 77, p. Chinese J. Phys. Available at: https://doi.org/https://doi.org/10.1016/j.cjph.2021.10.045.

Ali, L., Ali, B., Liu, X., *et al.* (2022). Analysis of bio-convective MHD Blasius and Sakiadis flow with Cattaneo-Christov heat flux model and chemical reaction', *Chinese*

Journal of Physics, 77: 1963–1975. Available at: https://doi.org/https: //doi.org/10.1016/j.cjph.2021.12.008.

Ali, L., Ghori, B. and Muhammad, B.A. (2022). Melting effect on Cattaneo–Christov and thermal radiation features for aligned MHD nanofluid flow comprising microorganisms to leading edge: FEM approach. *Computers & Mathematics with Applications*, 109: 260–269. Available at: https://doi.org/ https: //doi.org/10.1016/j.camwa. 2022. 01.009.

Bachok, N., Ishak, A. and Pop, I. (2011). On the stagnation-point flow towards a stretching sheet with homogeneous-heterogeneous reactions effects. *Commun Non-Lin Sci Numer Simulat*, 16: 4296–4302.

Chaudhary, M. and Merkin, J. (1996). Homogeneous-heterogeneous reactions in boundary-layer flow: effects of loss of reactant. *Math Comput Model*, 24: 21–28.

Hayat, T., Sumaira, Q., Maria, I. and Ahmed, A. (2016). Three-dimensional rotating flow of Jeffrey fluid for Cattaneo-Christov heat flux model. *American Institute of Physics* [Preprint]. Available at: https://doi.org/10.1063 /1. 4942091.

Hsiao, K. (2017). Combined electrical MHD heat transfer thermal extrusion system using Maxwell fluid with radiative and viscous dissipation effects, *Appl Therm Eng*, 112: 1281–1288.

Khan, N., Mahmood, T., Sajid, M., and Hashmi, M.S. (2016). Heat and mass transfer on MHD mixed convection axisymmetric chemically reactive flow of Maxwell fluid driven by exothermal and isothermal stretching disks, *Int J Heat Mass Transfer*, 92: 1090–1105.

Kumari, M., Grosan, T. and Pop, I. (2006). Rotating flow of Power-Law fluids over a stretching surface, *Tech Mech*, 26: 11–19.

Maqsood, N., Khan, A.J. and Mustafa, M. (2017). Numerical tackling for viscoelastic fluid flow in rotating frame considering homogeneous-heterogeneous reactions. *Results in Physics*, 7: 3475–3481. Available at: https://doi.org/3475-3481.

Marinca, V. Herișanu, N., Bota, C. and Marinca, B. (2009). An optimal homotopy asymptotic method applied to the steady flow of fourth-grade fluid past a porous plate, *Appl Math Lett*, 22: 245–251.

Merkin, J. (1996). A model for isothermal homogeneous-heterogeneous reactions in boundary-layer flow, *Math Comput Model*, 24: 125–136.

Mustafa, M., Khan, J.A., Hayat, T. and Alsaedi, A. (2015). Bodewadt flow and heat transfer of nanofluid over a stretching stationary disk, *J Mol Liq*, 211: 119–125.

Nazar, R., Amin, N. and Pop, I. (2004). Unsteady boundary layer flow due to a stretching surface in a rotating fluid, *Mech Research Commun.*, 31: 121–8.

Reddy, P. B. A., Suneetha, S., Subbarayudu, K., T.H. Al-Arabi, T.H., and A.M. Rashad, A.M. (2021). Exploration of physical features of homogeneous–heterogeneous chemical action in a nanofluid film dispensed with MOS2 in diathermic oils, *Journal of Taibah University for Science*, 15(1): 826–839. Available at: https://doi.org/DOI: 10.1080/16583655.2021.2004728.

Sen, S.S.S., Das, M. and Shaw, S. (2021). Thermal dispersed homogeneous-heterogeneous reaction within MHD flow of a Jeffrey fluid in the presence of Newtonian cooling and nonlinear thermal radiation. *Heat Transfer*, 50(6): 5744–5759. Available at: https://doi.org/https: //doi.org/10.1002/htj.22146.

Shafique, Z., Mustafa, M. and Mushtaq, A. (2016). Boundary layer flow of Maxwell fluid in rotating frame with binary chemical reaction and activation energy. *Results Phys*, 6: 627–33.

Shah, Z., Gul, T., Khan, M.A., Ali, I., Islam, S. and Husain, F. (2017). Effects of hall

current on steady three dimensional non-newtonian nanofluid in a rotating frame with brownian motion and thermophoresis effects. *Journal of Engineering Technology*, 6: 280–296.

Shah, Z., Islam, S., Gul, T., Bonyah, E. and Khan, M.A. (2018). The electrical MHD and Hall current impact on micropolar nanofluid flow between rotating parallel plates. *Results in Physics*, 9: 1201–1214.

Singh, V. and Agarwalb, S. (2014). MHD flow and heat transfer for Maxwell fluid over an exponentially stretching sheet with variable thermal conductivity. *Thermal Science*, 18(2): S599–S615.

Sravanthi, C.S. and Gorla, R.S.R. (2018). Effects of heat source/sink and chemical reaction on MHD Maxwell nanofluid flow over a convectively heated exponentially stretching sheet using homotopy analysis method. *Int J Applied Mechanics and Engineering*, 23(1): 137–159.

Turkyilmazoglu, M. (2012). MHD fluid flow and heat transfer due to a stretching rotating disk, *Int J Therm Sci*. 51: 195–201.

Turkyilmazoglu, M. (2014) 'Bodewadt flow and heat transfer over a stretching stationary disk', *Int J Mech Sci*, 90: 246–50.

Waini, I., Zainal, N.A. and Khashi, N.S. (2017). Aligned magnetic field effects on flow and heat transfer of the upper-convected Maxwell fluid over a stretching/shrinking Sheet, *MATEC Web of Conferences* [Preprint]. Available at: https://doi.org/10.1051/matecconf/20179701078.

Wang, C. (1988). Stretching a surface in a rotating fluid, *ZAMP*, 39: 177–85.

Zaimi, K., Ishak, A. and Pop, I. (2013). Stretching surface in rotating viscoelastic fluid, *Appl Math Mech*, 34: 945–952.